





An Unbalance and Power Controller Allowing Smooth Islanded Transitions in Three-Phase Microgrids

Andrea Lauri , Graduate Student Member, IEEE, Tommaso Caldognetto , Senior Member, IEEE, Davide Biadene , Member, IEEE, and Paolo Mattavelli , Fellow, IEEE

Abstract—This article introduces a power controller for three-phase inverters in microgrids that can be used in three-phase three-wire and three-phase four-wire systems. The controller enables active and reactive power tracking and unbalanced current control during grid-tied operation, while also allowing seamless transitions into islanded operation. The proposal is motivated by the compelling need in forthcoming power-electronics-dominated grids to provide ancillary services for the main grid and to support grid-forming functionalities for the microgrid, especially in case of islanded operation. The control is developed on the symmetrical components framework. Power tracking is achieved by dedicated control loops that, exploiting $P-f$ and $Q-V$ droop laws applied on positive-sequence powers, accommodate output-power control during grid-tied operation as well as grid-forming capabilities during islanded operation. The controller also includes synchronous dq -frame control for negative-sequence current regulation for providing unbalanced current compensation. The proposed solution addresses the challenge of simultaneously providing concurrent grid-tied control features, such as output power tracking, during grid-tied operation as well as grid-forming capabilities during islanded operation. The related challenge stems from the intrinsically different control actions involved in the two modes of operation, namely, grid tied and islanded. The proposal is verified on an experimental setup composed of converters rated 3 kW.

Index Terms—Droop control, grid-tied inverter, microgrid, symmetrical sequences, unbalanced voltage.

I. INTRODUCTION

THE rapidly evolving energy scenario and the related challenges foster the development of power electronic based

Manuscript received 23 March 2023; revised 21 June 2023 and 24 November 2023; accepted 14 December 2023. This work was carried out within the MOST-Sustainable Mobility Center and supported by the European Union Next-GenerationEU (PIANO NAZIONALE DI RIPRESA E RESILIENZA (PNRR) - MISSIONE 4 COMPONENTE 2, INVESTIMENTO 1.4 - D.D. 1033 17/06/2022, CN00000023). (Corresponding authors: Andrea Lauri; Tommaso Caldognetto.)

The authors are with the Department of Management and Engineering, University of Padova, 36100 Vicenza, Italy (e-mail: andrea.lauri@studenti.unipd.it; tommaso.caldognetto@unipd.it; davide.biadene@unipd.it; paolo.mattavelli@unipd.it).

Color versions of one or more figures in this article are available at <https://doi.org/10.1109/TIE.2023.3347836>.

Digital Object Identifier 10.1109/TIE.2023.3347836

power systems [1]. Microgrids play a pivotal role in this respect [2] since they represent a paradigm for the effective integration of distributed energy resources, such as renewables and energy storage systems, and the management of loads interfaced to the ac distribution system using electronic power converters (EPCs). Flexible power control is a crucial feature of EPCs in microgrids. It allows us to react to power references issued by controllers for local power flow optimizations [3], to provide demand-response services requested to the microgrid, or to participate in transactive energy markets [4], [5]. A second crucial feature is the availability of suitable EPC controllers endowing the microgrid capability of operating islanded from the main grid, which is valuable in several modern circumstances [6], [7]. Last, unbalanced current control should be included considering the control of fundamental quantities at the output of EPCs for power quality enhancements. This control flexibility can be exploited to compensate unbalanced currents measured at the connection with the upstream grid in three-phase systems populated by unbalanced or single-phase loads, which is a common issue in low-voltage grids. The outlined scenario is schematically represented in Fig. 1.

The analysis of the literature reveals that the cohesive integration of these features presents a relevant challenge. The main difficulty stems from the fundamentally different control requirements for grid-tied operation and islanded operation. In grid-tied operation, the goal of reference tracking must be achieved regardless of grid conditions. On the other hand, if disconnected from the mains, inverters must adapt to grid conditions to properly operate in parallel with other units and support the local grid voltage.

Droop control is widely used to implement grid-forming converters and achieve islanded operation capabilities. However, when droop control is applied, output power tracking is not automatically obtained, and controlling unbalanced output currents requires dedicated provisions. While current controllers [8] allow the most flexible control during grid-tied operation, the islanded operation is not supported. An example is provided in [9], in which a control for grid-tied converters is proposed that is capable of injecting unbalanced and harmonic currents, but it does not allow islanded operation. On the other hand, droop control approaches like [10] allow islanded operation but do not support unbalanced compensation. Similar limitations

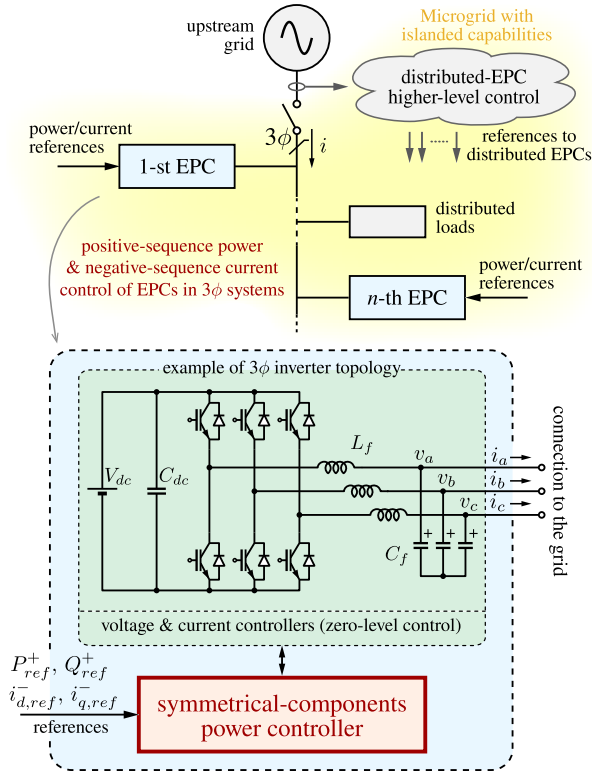


Fig. 1. Schematic overview of the future smart microgrid scenario.

can be found in [11] and [12]. In [13], a compensation method is proposed that allows to share the unbalanced power so that the total power on each phase is distributed among converters in proportion to their nominal power. Still, the additional flexibility of directly controlling the converters' contributions based on given references may be required for network optimizations [3], [14]. Several works discuss the concept of virtual synchronous machines, for example, [15], [16], [17]. In this case too, the capability of supporting phase-by-phase power control, to provide, for example, unbalanced compensation, coupled with the grid-forming function is typically not achieved. In [18] and [19], the virtual-oscillator control technique is modified to enhance the operation in three-phase unbalanced grids. Operation with distinct power references for each phase has not been shown.

Preliminary solutions to couple power control and islanded operation are documented in [20], where a total output power controller is proposed that also allows seamless transitions toward the islanded operation. As a prosecution of this work, output power control performed on the three-phases (i.e., per-phase) aiming at unbalance power compensation is introduced in [21] and [22]. In these papers, per-phase active and reactive power control in three-phase four-wire systems, the former, and three-wire systems, the latter, are tackled. The approach in these two articles, however, assumes that the unbalance compensation is performed providing unbalanced power, as shown in [23]. However, symmetrical-components give a more natural approach to unbalance compensation, as shown in [24], and allow a unique controller implementation for three-phase

EPCs with or without the neutral wires. Remarkably, three-wire systems with the neutral wire and also without the neutral wire are both relevant in low-voltage networks [25], and the controller proposed herein is compatible with both configurations.

Approaching the problem through a positive- and negative-sequence power controller would be ineffective. While, during normal operation, positive-sequence voltage has a well-defined and bounded amplitude value, this is not true for negative-sequence voltage. The negative-sequence power loop-gain would vary with the negative-sequence voltage amplitude, and may reduce to zero in case of perfectly balanced three-phase voltages. For this reason, droop control on negative-sequence powers cannot be performed as commonly done for positive-sequence powers. The solution proposed here controls positive-sequence powers, for active and reactive output power tracking, and injects negative-sequence currents, to provide unbalanced compensation, by generating a suitable negative-sequence voltage component. In the control, the active-power control loop is used to synchronize the generated voltages with the grid, exploiting the feature discussed in [26], and to derive the negative-sequence instantaneous phase used to regulate the injected negative-sequence currents. In summary, the proposed method includes the following key features:

- 1) active and reactive power tracking;
- 2) unbalance current regulation;
- 3) grid-forming capability;
- 4) parallel operation with multiple grid-forming units;
- 5) smooth and seamless transition toward islanded operation.

The rest of this article is organized as follows. Section II briefly reviews the main power flow relations, used in the following sections, in ac single- and three-phase systems; Section III describes the operating principles of the proposed approach and derives the small-signals loop gains; Section IV illustrates a basic design guideline for the controller parameters; Sections V and VI show, respectively, simulation and experimental results validating the control approach. Finally, Section VII concludes this article.

II. FUNDAMENTAL MODELING OF AC POWER TRANSFER

This section recalls the main power transfer relations between two voltage sources, representing the ac main grid and a voltage-controlled grid-tied inverter, in both single-phase and three-phase systems. It is assumed that the line impedance connecting the sources is mainly inductive; a related remark on this assumption is reported at the end of this section.

For a single-phase inverter connected to the ac main grid by an inductive line, the power flow equations can be written as [27], [28]

$$\dot{S} = \frac{V_i V_g}{\omega_g L} \sin(\varphi_i) + j \frac{V_g}{\omega_g L} [V_i \cos(\varphi_i) - V_g] \quad (1)$$

where $V_i \angle \varphi_i$ and $V_g \angle 0$ are, respectively, the inverter and the grid-voltage phasors and ω_g is the grid frequency. Assuming small φ_i and small $\Delta V_i \triangleq V_i - V_g$, by linearizing (1) it yields

$$P^+ \approx \gamma_p \varphi_i; \quad Q^+ \approx \gamma_q \Delta V_i \quad (2)$$

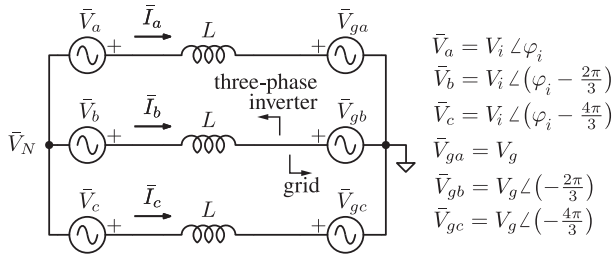


Fig. 2. Three-phase three-wires grid-connected inverter under balanced conditions.

where $\gamma_p \triangleq \frac{V_g^2}{\omega_g L}$ and $\gamma_q \triangleq \frac{V_g}{\omega_g L}$.

For three-phase four-wires connections (i.e., three-phase with neutral line), (1), (2) hold independently for each of the three phases of the inverter. However, when the neutral line is absent, as displayed in Fig. 2, the additional constraint $i_a + i_b + i_c = 0$ must be satisfied, thus preventing an independent power control of the three phases, namely, a per-phase power control. In [22], the implications of this constraint on the per-phase power flow are reported. Herein, the focus is on positive-sequence power flow; in this case, (1) and (2) can be written as

$$\dot{S} = 3 \frac{V_i V_g}{\omega_g L} \sin(\varphi_i) + 3j \frac{V_g}{\omega_g L} [V_i \cos(\varphi_i) - V_g] \quad (3)$$

$$P^+ \approx 3\gamma_p \varphi_i; \quad Q^+ \approx 3\gamma_q \Delta V_i. \quad (4)$$

These relations are considered in the following sections to describe the proposed controller.

It is worth remarking that the power-flow relations (4), holding with inductive interconnection impedances, allow the use of $P-f$ and $Q-V$ droop laws [28]. These laws are preferred, over other alternatives, because they allow accurate active power sharing, and they preserve the desirable active-power *versus* frequency relations characteristic of synchronous generators [29]. If necessary, the inductive behavior is commonly enforced through impedance emulation, by a suitable design of the EPC output voltage regulator, or by adding a dedicated virtual-impedance loop as done, for example, in [29], [30], and [31].

III. PROPOSED CONTROL TECHNIQUE

The proposed power controller allows the following:

- 1) the control of direct-sequence active and reactive powers;
- 2) the injection of negative-sequence currents for unbalanced load supply;
- 3) smooth and seamless transition to islanded operation.

Power control is achieved via droop control, which assumes in this case inductive line impedance. As discussed in Section II, this is an assumption commonly verified. Moreover, it is possible to enforce this condition via impedance emulation techniques.

A. Controller Structure

The controller can be divided into three sections, as shown in Fig. 3 and explained in the following.

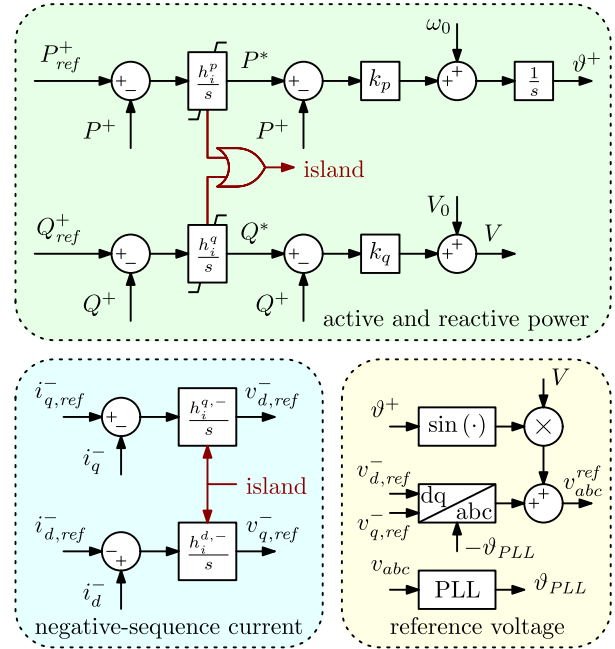


Fig. 3. Block scheme of the proposed controller.

1) Active and Reactive Power Controllers: first, the active power controller is composed of an inner loop that implements the classical $P-f$ droop characteristic

$$\omega = \omega_0 + k_p (P^* - P^+) \quad (5)$$

where ω_0 and ω are the reference and actual grid frequencies, k_p is the droop coefficient, P^* is the power reference, and P^+ is the direct-sequence measured active-power. Then, an outer control loop adjusts P^* to track the reference signal and achieve $P^+ = P_{ref}^+$. This loop is responsible for the synchronization with the instantaneous phase of the voltage at the point of connection of the EPC with the grid [26].

Similarly, the reactive power controller is composed of an inner loop that implements the $Q-V$ droop characteristic

$$V = V_0 + k_q (Q^* - Q^+) \quad (6)$$

where V_0 and V are the reference and the actual grid voltages, respectively, k_q is the droop coefficient, Q^* is the power reference, and Q^+ is the measured direct-sequence reactive power. Then, an outer control loop adjusts Q^* to track the given reference signal and achieve $Q^+ = Q_{ref}^+$. Then, the positive-sequence voltage reference is defined by the instantaneous phase given by the active power controller and the voltage amplitude given by the reactive power controller.

The small-signals block diagrams for the active and reactive power loops are shown in Fig. 4(a) and (b). The loop gains can be written as

$$T_{P^+}(s) = \frac{h_i^p}{s} \cdot \frac{3\gamma_p k_p H_{pm}(s)}{s + 3\gamma_p k_p H_{pm}(s)} \quad (7)$$

$$T_{Q^+}(s) = \frac{h_i^q}{s} \cdot \frac{3\gamma_q k_q H_{pm}(s)}{1 + 3\gamma_q k_q H_{pm}(s)} \quad (8)$$

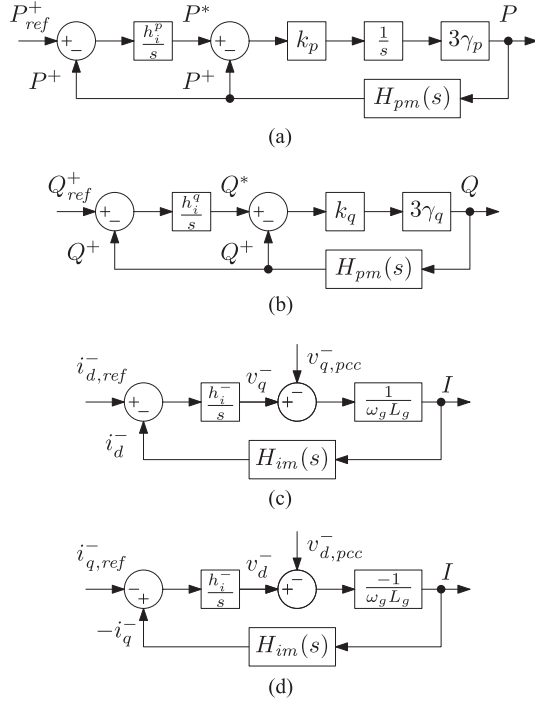


Fig. 4. Small-signals block schemes of a grid-tied converter controlled with the proposed method. (a) and (b) Active and reactive power loops, (c) and (d) negative-sequence current loops.

where $3\gamma_p$ and $3\gamma_q$, as defined in (4), are plant parameters describing the inverter response to phase-shift and voltage amplitude variations, while $H_{pm}(s)$ models the dynamics of the power measurement.

2) Negative-Sequence Currents Controller: This controller adds a negative-sequence voltage component to the reference produced by the power controllers, in order to enforce the flow of a set negative-sequence current that can be exploited for unbalance control. Assuming inductive line impedances, the voltages v_d^- and v_q^- , together with the components $v_{d,pcc}^-$ and $v_{q,pcc}^-$ at the point of common coupling (PCC), determine the negative-sequence current, as represented in Fig. 4(b) and (c). Herein, a clockwise rotating instantaneous phase, where d -axis is leading the q -axis, is used. From the scheme, considering the PCC voltage as an exogenous input, the loop gains of the negative-sequence current controller are

$$T_{i_d^-}(s) = -\frac{h_i^{q,-}}{s} \cdot \frac{1}{\omega_g L_g} \cdot H_{im}(s) \quad (9)$$

$$T_{i_q^-}(s) = \frac{h_i^{d,-}}{s} \cdot \frac{1}{\omega_g L_g} \cdot H_{im}(s)$$

where $1/(\omega_g L_g)$ represents the plant, that is, the dq impedance seen by the converter when injecting negative-sequence components.

3) Reference Voltage Generation: The generation of the voltage reference v_{abc}^{ref} is built by adding the contribution from the active and reactive power controller and the negative-sequence

current controller. The former contribution constitutes the positive sequence component of the voltage reference; it presents amplitude V and instantaneous phase ϑ^+ . The latter contribution constitutes the negative sequence component of the voltage reference and it is derived from the components $v_{d,ref}^-$ and $v_{q,ref}^-$. It is worth remarking that the final reference provided by the proposed controller is a voltage reference for the EPCs, which are always controlled as voltage sources.

B. Grid-Tied Operation

During grid-tied operation EPC output power regulation is physically possible, because the presence of the main grid ensures the presence of a slack node that can supply the mismatch among the power absorbed by the loads and the generation by the distributed EPCs [32]. The integrators in the active and reactive power loops will adjust the reference values P^* and Q^* in order to set the output power to the reference values P_{ref}^+ , Q_{ref}^+ . This is needed in case the grid-voltage frequency and amplitude are differ from the nominal value.

The negative-sequence instantaneous phase is computed using a phase-locked loop (PLL) fed with the output capacitor voltages v_a , v_b , v_c and providing the phase ϑ_{PLL} , as shown in Fig. 3. In fact, the phase ϑ^+ may differ from the phase of the actual output voltages due to the implemented virtual output impedances and the nonideality of the voltage regulator.

Active and reactive power reference values, together with negative-sequence current ones, are provided externally with respect to this controller, as foreseen in the scenario represented in Fig. 1.

C. Islanded Transition and Operation

When the main grid disconnects, the conditions highlighted at the beginning of Section III-B decay, and the generated power within the microgrid must automatically match loads consumption. Being power regulation no more possible, the power regulation error increases, leading the integrators in the power regulation loop to saturate. Eventually, the system enters islanded operation with fixed droop characteristics

$$\begin{cases} \omega = \omega_0 + k_p (P_{sat}^* - P_d) \\ V = V_0 + k_q (Q_{sat}^* - Q_d) \end{cases} \quad (10)$$

which allows automatic load sharing among the EPCs connected to the islanded microgrid. The transition, from the point of view of the output voltage, happens in a smooth and seamless way. When at least one integrator reaches saturation, a reset signal is sent to the negative-sequence current controller, disabling it. Remarkably, the island detection is performed independently by each inverter, so that no coordination is needed, neither among converters nor toward a centralized controller.

IV. CONTROLLER DESIGN

The main equations for the design of the controller are derived in this section, and the design process is discussed, starting from the choice of the saturation thresholds, through the design of the

power regulation loops, to the negative-sequence current loops design.

A. Droop Coefficients and Saturation Thresholds

Droop coefficients can be chosen in various ways, and in general there is a tradeoff between the error in the drooped quantities and the speed of the dynamic response of the system. A simple design procedure is to consider the nominal power of the inverter S_N (assuming to be both nominal absorbed and supplied output power) and the width of the interval in which ω and V can vary, then

$$k_p = \frac{\omega_{\max} - \omega_{\min}}{2S_N}; \quad k_q = \frac{V_{\max} - V_{\min}}{2S_N} \quad (11)$$

as it is commonly done. More sophisticated methods exist, allowing the investigation of small-signals behavior of multiple parallel-connected droop-controlled ac sources, like, for example, [33], [34].

Once droop coefficients are determined, it is possible to define the saturation values for the integrators in the power loops. Starting with the active power, from (5) it is possible to write

$$P^* = \frac{\omega - \omega_0}{k_p} + P^+$$

which is the droop characteristic reference value needed to generate a particular value P^+ of active power when the actual grid frequency is ω . By knowing the minimum and maximum ω value of the tolerable grid frequency and the maximum and minimum P^+ that the inverter can generate (or absorb), it is possible to find

$$P_{\min}^* = \frac{\omega_{\min} - \omega_0}{k_p} - S_N; \quad P_{\max}^* = \frac{\omega_{\max} - \omega_0}{k_p} + S_N. \quad (12)$$

Similarly for Q^* , from (6)

$$Q^* = \frac{V - V_0}{k_q} + Q^+$$

then

$$Q_{\min}^* = \frac{V_{\min} - V_0}{k_q} - S_N; \quad Q_{\max}^* = \frac{V_{\max} - V_0}{k_q} + S_N \quad (13)$$

by knowing V_{\min} , V_{\max} , Q_{\min} , and Q_{\max} . It is worth remarking that, in order to track all the references for the reactive power, it may be necessary to extend the considered thresholds, as voltage amplitude is not the same along the whole microgrid.

B. Power Regulation Loops

The active-power loop and the reactive-power loop have different dynamic behavior, because the former includes an additional pole in the origin due to the integrator computing the instantaneous-phase signal ϑ .

From (7), the value of h_i^p can be chosen based on desired specifications of control bandwidth and phase margin. Neglecting the power measurement dynamics $H_{\text{pm}}(s)$, initial licit solutions are $h_i^p = 3\gamma_p k_p / 4$, to achieve a critically damped (i.e., coincident real poles) closed-loop transfer function, or $h_i^p = 3\gamma_p k_p / 2$, to achieve a second-order Butterworth poles placement (i.e., $\xi = 1/\sqrt{2}$).

For what concerns the reactive-power loop, it is possible to achieve wider control bandwidths, which are limited only by the power measurement block while the process to be regulated is static. Considering (8), and neglecting the dynamics of the power measurement, one can write

$$T_{Q^+}(s) = \frac{h_i^q}{s} \cdot \frac{3\gamma_q k_q}{1 + 3\gamma_q k_q} = \frac{h_i^q}{s} A_{Q^+}$$

and then choose $h_i^q = \omega^* / A_{Q^+}$ where ω^* is the target bandwidth, which, for example, may be set to match the active-power loop bandwidth.

C. Negative-Sequence Current Loop

The negative-sequence current regulation is performed by decomposing the currents into symmetrical components, using a reference frame synchronized with the instantaneous phase ϑ^- provided by the PLL. As discussed in the previous section, i_d^- is regulated adding a v_q^- component, while i_q^- by adding a v_d^- component. From (9), and neglecting the current decomposition dynamics, the design is straightforward. For example, the target bandwidth ω^* can be set first and, subsequently, choose $h_i^{q,-} = h_i^{d,-} = \omega^* \omega_g L_g$.

D. Poles Trajectories

Fig. 5 shows the poles trajectories of the closed-loop system with respect to the design of the outer integral regulator. In particular, Fig. 5 shows the closed-loop pole locations of the active-power loop (7) as h_i^p is varied. The same is shown in Fig. 5(b) for the reactive-power loop (8), varying h_i^q . Similarly, the location of the poles for negative-sequence current-loops are shown, assuming the same regulator gain h_i^- for both loops (9). The power measurement and current decomposition dynamics are considered to be first-order filters, as follows:

$$H_{\text{pm}}(s) = \frac{1}{1 + s/\omega_{\text{pm}}}; \quad H_{\text{im}}(s) = \frac{1}{1 + s/\omega_{\text{im}}}. \quad (14)$$

V. SIMULATION RESULTS

The proposed controller has been validated by simulation results, discussed in this section, and experimental results, discussed in Section VI. The simulation results are carried out in order to validate the parallel operation of two inverters implementing the proposed control method.

The test is devised to validate all the capabilities of the proposed method, namely, the following:

- grid-tied operation;
- active power reference tracking;
- reactive power reference tracking;
- unbalance current compensation at the PCC;
- transition into islanded operation;
- islanded operation.

In the test, two inverters are connected in parallel and initially operating in grid-tied mode. The two inverters have identical control parameters, reported in Table II. Two different loads are connected at the PCC, namely, an unbalanced three-phase Y resistive load, composed of two 10 Ω and one 30 Ω resistors,

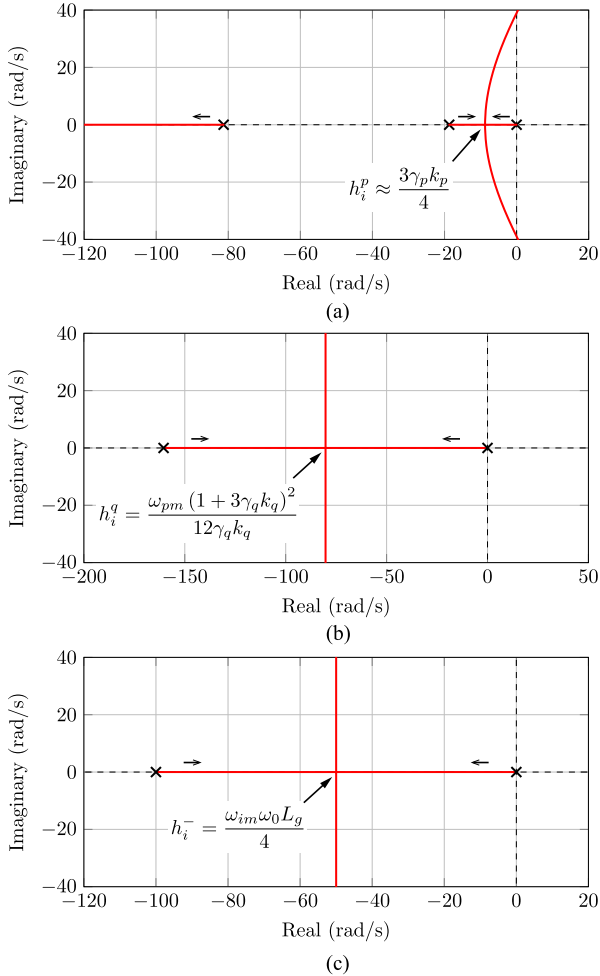


Fig. 5. Trajectories of the closed-loop poles varying the design of the integral regulators. (a) Trajectories for active-power loop (7), (b) for reactive-power loop (8), and (c) for negative-sequence current loops (9). The power measurement and current decomposition dynamics are assumed to be first-order low-pass filters, with cut-off frequencies, respectively, ω_{pm} and ω_{im} , as shown in (14).

TABLE I
INVERTER AND GRID PARAMETERS

Parameter	Value
DC-link voltage	V_{dc} 370 V
Switching frequency	f_{sw} 50 kHz
Output filter inductor	L_f 340 μ H
Output filter capacitor	C_f 5.7 μ F
Nominal power rating	S_N 3 kVA
Grid frequency	ω_g $2\pi \cdot 50$ rad/s
Grid rms voltage	V_g 110 V
Line impedance	Z_{line} 26.6 m Ω , 48 μ H

and a balanced three-phase Y capacitive load, composed of three 100 μ F capacitors. The test scenario corresponds to the one depicted in Fig. 1, assuming $n = 2$.

Fig. 6 reports the main quantities of the EPCs along the performed test and a table that describes the succession of events. From top to bottom, the left side of Fig. 6 displays active powers, reactive powers, and the current amplitudes at the PCC; the right side of Fig. 6 displays the grid frequency, the voltage measured

TABLE II
CONTROLLER PARAMETERS

Parameter	Value
Inductive output impedance	L_g 3.18 mH
P - f droop coefficient	k_p 0.419 mrad/W \cdot s
Q - V droop coefficient	k_q 1.83 mV/VAr \cdot s
Active-power integral gain	h_i^p 5 1/s
Reactive-power integral gain	h_i^q 30 1/s
Negative-sequence curr. int. gain	h_i^- 6.28 Ω /s
Active power sat.	$P_{max,min}^*$ ± 4.5 kW
Reactive power sat.	$Q_{max,min}^*$ ± 4.5 kVar
Negative-sequence volt. sat.	$v_{max,min}^-$ ± 15 V
Frequency reference value	ω_0 $2\pi \cdot 50$ rad/s
Voltage reference rms value	V_0 110 V

at the output of an EPC and the instantaneous PCC voltage across the disconnection from the main grid disconnection, which happens at $t = 15$ s. Steps of power references are applied during intervals b), considering active power, and c), considering reactive power. Interval d) shows the unbalanced current control capability of the proposed controller exploited with the goal of compensating the unbalanced current at the PCC. To this end, the negative-sequence currents at the PCC are measured and then used as reference for the signals $\bar{i}_{q,ref}^-$ and $\bar{i}_{d,ref}^-$. The reference signals are set at the same value for EPC₁ and EPC₂, equal to half of the negative-sequence currents initially measured at the PCC, in order to evenly share the compensation effort; remarkably, the measured current during this interval d) are balanced, as desired and expected based on the set references. In e), at $t = 15$ s, the main grid is disconnected. The two inverters start the transition to islanded operation, which is completed at the beginning of f), at $t = 22.2$ s.

VI. EXPERIMENTAL RESULTS

The proposed controller has been validated experimentally under different operating conditions. The results reported in the following were obtained using the experimental setup displayed in Fig. 7. It includes two EPCs, implemented by using a rapid prototyping system that is described in detail in [35]. Each EPC embeds an ImperixBBoard Pro digital controller and three half-bridge power boards based on 600-V, 50-m Ω GaN FETs by Texas Instruments (LMG341xR050). Each EPCs is supplied by a dedicated power supply Keysight RP7962 A. The upstream main grid is emulated by a Cinergia ac voltage source, model GE/EL+20 vAC/DC. Data acquisition is performed by Dewesoft SIRIUSi digital acquisition systems. The parameters of the EPCs as defined in Fig. 1 are listed in Table I, and control parameters are listed in Table II.

In the following, three test configurations are reported, namely, Section VI-A power regulation in grid-connected operation with balanced load plus a transition toward islanded operation, Section VI-B negative-sequence current regulation for supplying an unbalanced three-phase load plus a transition toward islanded operation, Section VI-C power and unbalance regulation of two parallel-connected inverters connected to a grid with unbalanced voltages plus a transition toward islanded operation. The first two configurations are meant to show the

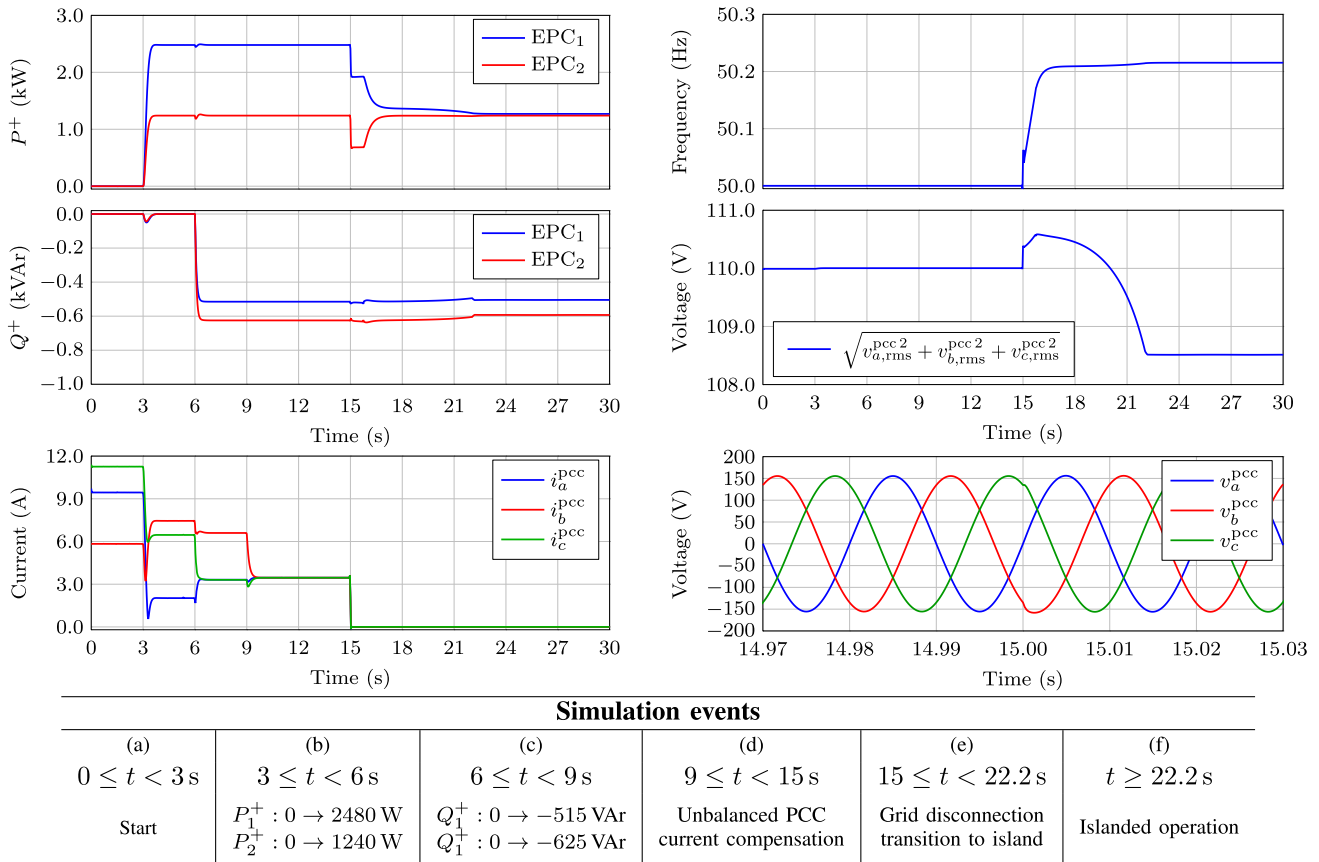


Fig. 6. Simulation test with two parallel-operating inverters, initially operating in grid-tied condition. Unbalanced three-phase Y load is connected at the PCC, composed of two 10Ω and one 30Ω resistors, and three $100 \mu\text{F}$ capacitors. Nomenclature as in Fig. 1. The sequence of events (a)–(f) is described in the table on the bottom.

principle of operation of the controller in a simple application example with a single EPC. The third configuration shows the operation of the controller in a more realistic condition and considers two EPCs.

A. Power Regulation With a Single Inverter

In this test, a three-phase inverter, namely, EPC 1, is tied to the three-phase ac grid; EPC 2 is disconnected. A three-phase balanced 27Ω resistive load is locally connected. The main waveforms are shown in Fig. 8, which reports the direct-sequence active and reactive powers, the rms values of output voltage and current, and the frequency. Initially, both P_{ref}^+ and Q_{ref}^+ reference values are equal to zero. At $t = 6.2$ s, a step change $P_{\text{ref}}^+ : 0 \text{ W} \rightarrow 2.4 \text{ kW}$ is performed, and at $t = 9.2$ s the inverse step change $P_{\text{ref}}^+ : 2.4 \text{ kW} \rightarrow 0 \text{ W}$ is applied. At $t = 12.2$ s the same step change is done for $Q_{\text{ref}}^+ : 0 \text{ VAr} \rightarrow 2.4 \text{ kVAr}$, and then again $Q_{\text{ref}}^+ : 2.4 \text{ kVAr} \rightarrow 0 \text{ VAr}$. The first graph in Fig. 8 shows that the system correctly tracks the given power reference values. At $t = 19.6$ s, the grid is disconnected by opening the circuit breaker CB in Fig. 7 and the EPC automatically initiates its transition to the island operation. Being some active power absorbed by the local load, the output frequency decreases until the integrator in the active-power regulation loop saturates. Similarly, a small value of reactive power is absorbed by the

system, thus, the integrator in the reactive power loop saturates too toward its upper limit. After $t \geq 23$ s, the system operates with a fixed droop characteristic.

B. Unbalance Regulation With a Single Inverter

In this test, an unbalanced three-phase load is connected to the grid. EPC 1 is connected, while EPC 2 is disconnected. The load is constituted of a 108Ω resistive load connected between phase b and phase c only. Fig. 9 shows the negative sequence d -axis and q -axis currents for the grid and for the EPC, and the grid rms current values. Initially, the unbalanced load is supplied by the grid, both in balanced and unbalanced components: the positive-sequence power and negative-sequence current references of the EPC are set to zero. At $t = 14.5$ s, a step-change in the negative-sequence current references is performed, in order to compensate the negative-sequence current absorbed by the load. Remarkably, for $15 \text{ s} \leq t \leq 25 \text{ s}$, the grid current is mainly a positive sequence current; in fact, the EPC supplies only negative-sequence components, whilst the positive-sequence power is still supplied by the grid. At $t = 25.5$ s, the grid is disconnected, and the load is entirely supplied by the EPC. The EPC performs its transition toward island operation as in the previous test.

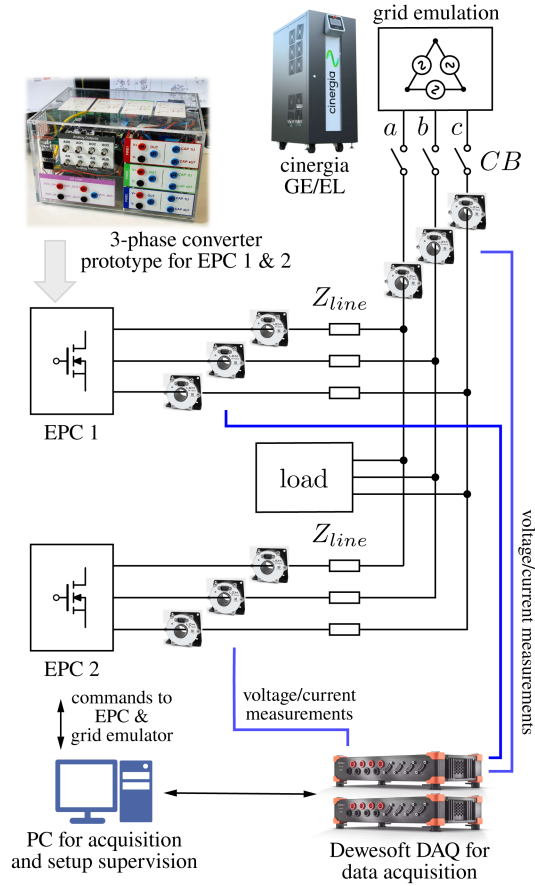


Fig. 7. Scheme of the experimental setup.

C. Multiple Inverters Operating in an Unbalanced Scenario

In this test, an unbalanced three-phase load is connected to the grid. The load is constituted of a $108\ \Omega$ resistive load connected between phase b and phase c only. The grid voltage is unbalanced, with an unbalance factor equal to 2.5%, defined as the magnitude ratio of negative-sequence to positive-sequence voltage. Both EPC 1 and EPC 2 are connected and controlled with the proposed method. The experimental waveforms are shown in Figs. 10 and 11.

Initially, both the inverters are set to zero output power and unbalanced current. At $t = 5\text{ s}$, a step of active power reference is applied to both the EPCs, such that $P_{\text{ref},1}^+ : 0\text{ W} \rightarrow 600\text{ W}$, and $P_{\text{ref},2}^+ : 0\text{ W} \rightarrow 900\text{ W}$. The EPCs track the given power references and, as expected, the provided phase currents are all balanced. At $t = 8\text{ s}$, the negative-sequence current references are set to compensate the unbalanced current absorbed by the grid. This means $i_{q,\text{ref},1}^- : 0\text{ A} \rightarrow -0.84\text{ A}$, and $i_{q,\text{ref},2}^- : 0\text{ A} \rightarrow -0.6\text{ A}$. Remarkably, even in an unbalanced scenario, the controller is capable of regulating the positive-sequence power and negative-sequence currents with the same dynamical performances as in the balanced case. At $t \approx 16\text{ s}$, the main grid

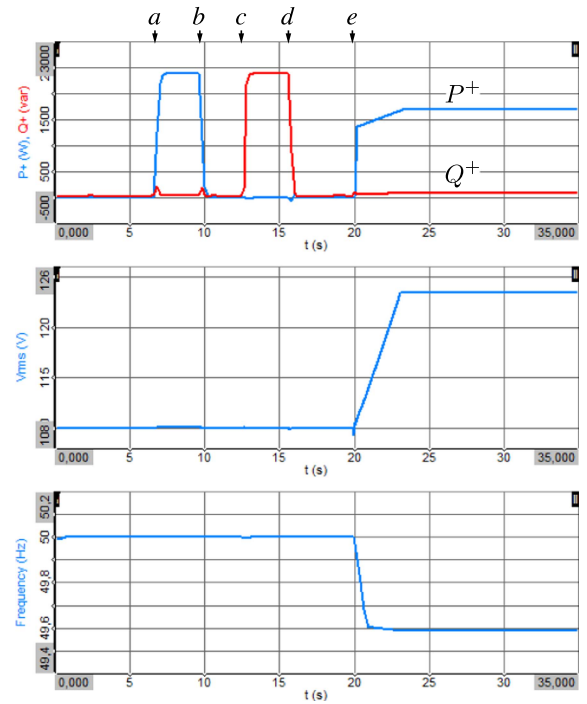


Fig. 8. Experimental waveforms for the power regulation test. (a) $P^+ : 0 \rightarrow 2.4\text{ kW}$; (b) $P^+ : 2.4\text{ kW} \rightarrow 0$; (c) $Q^+ : 0 \rightarrow 2.4\text{ kVAR}$; (d) $Q^+ : 2.4\text{ kVAR} \rightarrow 0$; (e) disconnection from the main grid. With symmetrical PCC voltages, P^+ , Q^+ equal total active and reactive powers.

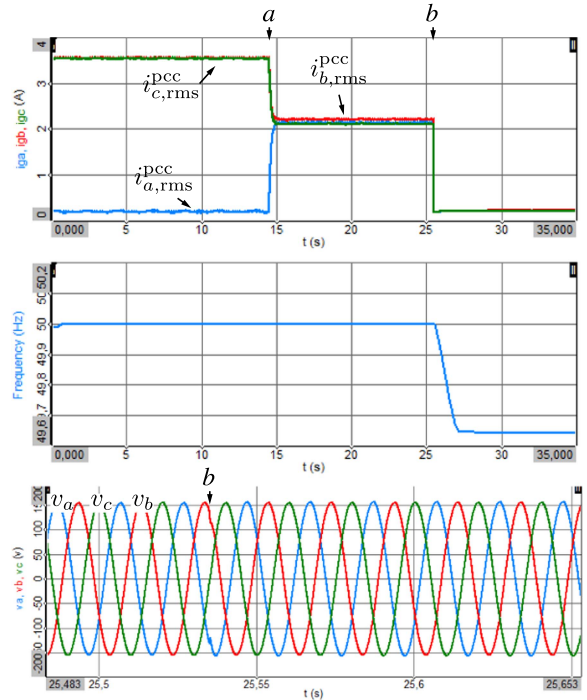


Fig. 9. Experimental waveforms showing unbalanced compensation capabilities of the proposed controller. (a) $i_{d,q}^-$ are set to compensate unbalanced current flow at PCC; (b) disconnection from the main grid. Bottom figure shows clean voltage waveforms at (b).

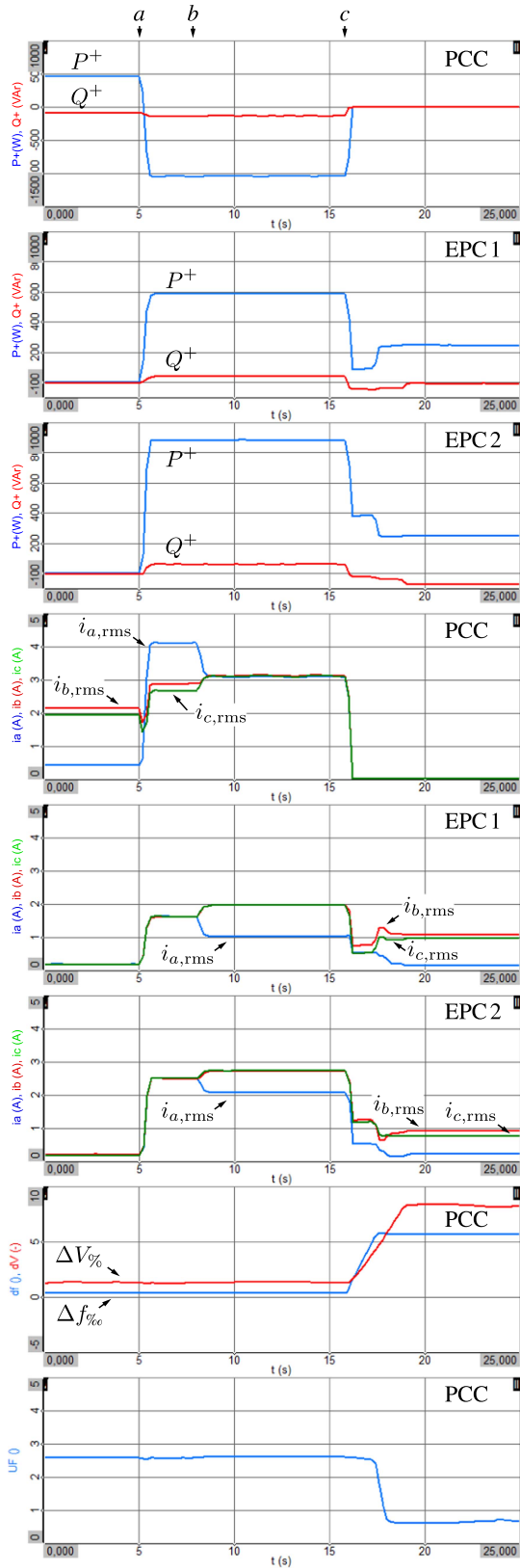


Fig. 10. Experimental tests with two grid-tied inverters: (a) $P_1^+ : 0 \rightarrow 600 \text{ W}$, $P_2^+ : 0 \rightarrow 900 \text{ W}$; (b) Unbalance compensation; (c) Main grid disconnection and islanded operation.

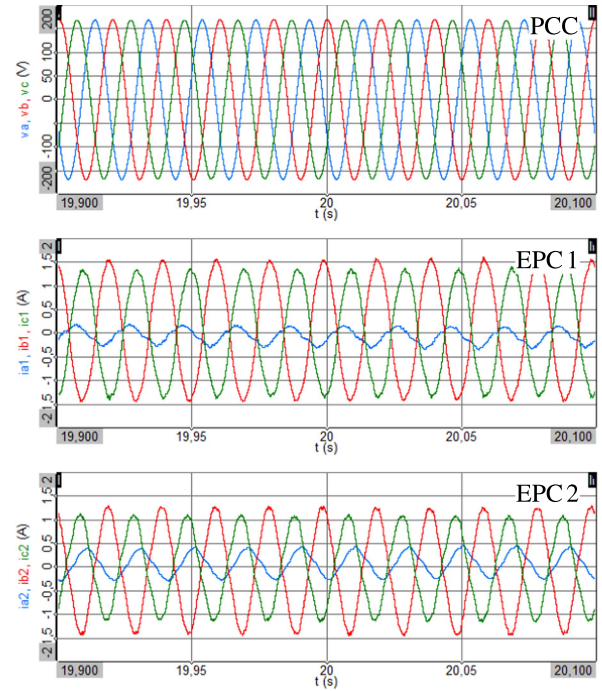


Fig. 11. Experimental waveforms showing the islanded operation in Fig. 10 around $t = 20 \text{ s}$.

is disconnected, by opening the circuit breaker CB displayed in Fig. 7. The inverters are involved in the transition toward islanded operation, which is completed at around $t \approx 17.5 \text{ s}$ when the integrators in the power loops reach saturation levels. At this point, the negative-sequence current loop is disabled. This creates a transient visible on the inverters rms currents in the time interval $17.5 \text{ s} \leq t \leq 18.5 \text{ s}$. Subsequently, the system reaches a steady state and the transition can be considered complete. Voltage waveforms taken around $t = 20 \text{ s}$ are shown in Fig. 9, to prove the stability among multiple grid-forming inverters connected together.

VII. CONCLUSION

A controller capable of regulating positive-sequence powers and negative-sequence currents at the output of grid-tied inverters, also allowing seamless transitions into islanded operation, was proposed. The control approach conjugates flexible power control and unbalance compensation, during grid-tied operation, with the capability to adapt to the microgrid needs, during islanded operation. A simple yet effective design procedure was reported, which can be further tailored to comply with specific control requirements. The approach was tested considering an experimental power electronic system composed of two inverters. Simulation and experimental results demonstrated the control performance of the proposed controller and its capability to smoothly transition into islanded operation, even in the presence of unbalanced loads, unbalanced grid voltages, and multiple converters operating in parallel with the proposed controller. To summarize, the proposed solution:

- 1) integrates power control and unbalanced currents control with seamless islanded transitions;
- 2) showed proper operation in unbalanced grid conditions;
- 3) was demonstrated experimentally to support islanded operation when applied to multiple parallel-connected grid-forming converters.

The solution finds applications in microgrid inverters controllers to implement active and reactive power control, unbalanced power control, and islanded operation capability of distributed three-phase inverters. Remarkably, the approach is applicable to both three-wire and four-wire systems; besides, in the latter case, it is possible to add a further loop for controlling the output homopolar current of the EPC.

ACKNOWLEDGMENT

This article reflects only the authors views and opinions, neither the European Union nor the European Commission can be considered responsible for them.

REFERENCES

- [1] IEA, "World energy outlook 2022," IEA, Paris, France, Rep., 2022. [Online]. Available: <https://www.iea.org/reports/world-energy-outlook-2022>
- [2] R. Panigrahi, S. K. Mishra, S. C. Srivastava, and P. Enjeti, "Microgrid integration in smart low-voltage distribution systems," *IEEE Power Electron. Mag.*, vol. 9, no. 2, pp. 61–66, Jun. 2022.
- [3] P. Tenti and T. Caldognetto, "Integration of local and central control empowers cooperation among prosumers and distributors towards safe, efficient, and cost-effective operation of microgrids," *Energies*, vol. 16, no. 5, 2023, Art. no. 2320.
- [4] P. Siano, G. De Marco, A. Rolán, and V. Loia, "A survey and evaluation of the potentials of distributed ledger technology for peer-to-peer transactive energy exchanges in local energy markets," *IEEE Syst. J.*, vol. 13, no. 3, pp. 3454–3466, Sep. 2019.
- [5] M. Khorasany, A. Najafi-Ghalelou, and R. Razzaghi, "A framework for joint scheduling and power trading of prosumers in transactive markets," *IEEE Trans. Sustain. Energy*, vol. 12, no. 2, pp. 955–965, Apr. 2021.
- [6] S. Chandak and P. K. Rout, "Microgrids during the outbreak of COVID-19," *IEEE Smart Grid Newslett.*, 2020.
- [7] K. Prabakar, "Microgrids-Support for the electric grid during natural disasters [Essay]," *IEEE Potentials*, vol. 42, no. 1, pp. 51–52, Jan./Feb. 2023.
- [8] A. Timbus, M. Liserre, R. Teodorescu, P. Rodriguez, and F. Blaabjerg, "Evaluation of current controllers for distributed power generation systems," *IEEE Trans. Power Electron.*, vol. 24, no. 3, pp. 654–664, Mar. 2009.
- [9] Z. Ali, N. Christofides, L. Hadjidemetriou, and E. Kyriakides, "Diversifying the role of distributed generation grid-side converters for improving the power quality of distribution networks using advanced control techniques," *IEEE Trans. Ind. Appl.*, vol. 55, no. 4, pp. 4110–4123, Jul./Aug. 2019.
- [10] Q.-C. Zhong and Y. Zeng, "Universal droop control of inverters with different types of output impedance," *IEEE Access*, vol. 4, pp. 702–712, 2016.
- [11] M. Karimi-Ghartemani, S. A. Khajehoddin, P. Piya, and M. Ebrahimi, "Universal controller for three-phase inverters in a microgrid," *IEEE Trans. Emerg. Sel. Topics Power Electron.*, vol. 4, no. 4, pp. 1342–1353, Dec. 2016.
- [12] X. Meng, Z. Liu, H. Zheng, and J. Liu, "A universal controller under different operating states for parallel inverters with seamless transfer capability," *IEEE Trans. Power Electron.*, vol. 35, no. 9, pp. 9794–9812, Sep. 2020.
- [13] E. Espina, M. Espinoza, and R. Cárdenas, "Active power angle droop control per phase for unbalanced 4-wire microgrids," in *Proc. IEEE Southern Power Electron. Conf.*, 2017, pp. 1–6.
- [14] D. I. Brandao, L. S. Araujo, A. M. S. Alonso, G. L. dos Reis, E. V. Liberado, and F. P. Marafão, "Coordinated control of distributed three- and single-phase inverters connected to three-phase three-wire microgrids," *IEEE Trans. Emerg. Sel. Topics Power Electron.*, vol. 8, no. 4, pp. 3861–3877, Dec. 2020.
- [15] S. A. Khajehoddin, M. Karimi-Ghartemani, and M. Ebrahimi, "Grid-supporting inverters with improved dynamics," *IEEE Trans. Ind. Electron.*, vol. 66, no. 5, pp. 3655–3667, May 2019.
- [16] V. L. Srinivas, B. Singh, and S. Mishra, "Self-synchronizing VSM with seamless operation during unintentional islanding events," *IEEE Trans. Ind. Informat.*, vol. 16, no. 9, pp. 5680–5690, Sep. 2020.
- [17] M. Ashabani and J. Jung, "Synchronous voltage controllers: Voltage-based emulation of synchronous machines for the integration of renewable energy sources," *IEEE Access*, vol. 8, pp. 49497–49508, 2020.
- [18] R. Ghosh, N. R. Tummuru, and B. S. Rajpurohit, "Modified VOC using three symmetrical components for grid-supporting operation during unbalanced grid voltages and grid-forming operation in hybrid single-phase/three-phase microgrid," *IEEE Trans. Ind. Electron.*, vol. 70, no. 11, pp. 11276–11286, Nov. 2023.
- [19] R. Ghosh, N. R. Tummuru, and B. S. Rajpurohit, "A new virtual oscillator-based grid-forming controller with decoupled control over individual phases and improved performance of unbalanced fault ride-through," *IEEE Trans. Ind. Electron.*, vol. 70, no. 12, pp. 12465–12474, Dec. 2023.
- [20] S. Lissandron and P. Mattavelli, "A controller for the smooth transition from grid-connected to autonomous operation mode," in *Proc. IEEE Energy Convers. Congr. Expo.*, 2014, pp. 4298–4305.
- [21] T. Caldognetto, H. Abedini, and P. Mattavelli, "A per-phase power controller for smooth transitions to islanded operation," *IEEE Open J. Power Electron.*, vol. 2, pp. 636–646, 2021, doi: [10.1109/OJPEL.2021.3134714](https://doi.org/10.1109/OJPEL.2021.3134714).
- [22] A. Lauri, H. Abedini, D. Biadene, T. Caldognetto, and P. Mattavelli, "Analysis of a droop-based power controller for three-phase microgrids," in *Proc. IEEE 24th Eur. Conf. Power Electron. Appl.*, 2022, pp. 1–8.
- [23] H. Abedini, T. Caldognetto, P. Mattavelli, and P. Tenti, "Real-time validation of power flow control method for enhanced operation of microgrids," *Energies*, vol. 13, no. 22, 2020, Art. no. 5959.
- [24] S. Acharya, M. S. El-Moursi, A. Al-Hinai, A. S. Al-Sumaiti, and H. H. Zeineldin, "A control strategy for voltage unbalance mitigation in an islanded microgrid considering demand side management capability," *IEEE Trans. Smart Grid*, vol. 10, no. 3, pp. 2558–2568, May 2019.
- [25] K. Strunz et al., *TF C6.04.02:TB 575—Benchmark Systems for Network Integration of Renewable and Distributed Energy Resources.*, Paris, France: Cigré, 2014.
- [26] Q. Zhong and D. Boroyevich, "Structural resemblance between droop controllers and phase-locked loops," *IEEE Access*, vol. 4, pp. 5733–5741, 2016.
- [27] K. De Brabandere, B. Bolsens, J. Van den Keybus, A. Woyte, J. Driesen, and R. Belmans, "A voltage and frequency droop control method for parallel inverters," *IEEE Trans. Power Electron.*, vol. 22, no. 4, pp. 1107–1115, Jul. 2007.
- [28] W. Yao, M. Chen, J. Matas, J. M. Guerrero, and Z.-M. Qian, "Design and analysis of the droop control method for parallel inverters considering the impact of the complex impedance on the power sharing," *IEEE Trans. Ind. Electron.*, vol. 58, no. 2, pp. 576–588, Feb. 2011.
- [29] Y. R. Li, F. Nejabatkhah, and H. Tian, *Smart Hybrid AC/DC Microgrids: Power Management, Energy Management, and Power Quality Control.*, Hoboken, NJ, USA: Wiley, 2022.
- [30] J. M. Guerrero, Luis Garcia de Vicuna, J. Matas, M. Castilla, and J. Miret, "Output impedance design of parallel-connected UPS inverters with wireless load-sharing control," *IEEE Trans. Ind. Electron.*, vol. 52, no. 4, pp. 1126–1135, Aug. 2005.
- [31] J. He and Y. W. Li, "Analysis, design, and implementation of virtual impedance for power electronics interfaced distributed generation," *IEEE Trans. Ind. Appl.*, vol. 47, no. 6, pp. 2525–2538, Nov./Dec. 2011.
- [32] M. B. Delghavi and A. Yazdani, "A unified control strategy for electronically interfaced distributed energy resources," *IEEE Trans. Power Del.*, vol. 27, no. 2, pp. 803–812, Apr. 2012.
- [33] S. Lissandron, A. Costabeber, and P. Mattavelli, "A generalized method to analyze the small-signal stability for a multi-inverter islanded grid with droop controllers," in *Proc. IEEE 15th Eur. Conf. Power Electron. Appl.*, 2013, pp. 1–10.
- [34] E. Coelho, P. C. Cortizo, and P. F. D. Garcia, "Small-signal stability for parallel-connected inverters in stand-alone AC supply systems," *IEEE Trans. Ind. Appl.*, vol. 38, no. 2, pp. 533–542, Mar./Apr. 2002.
- [35] T. Caldognetto et al., "A flexible power electronic converter system with rapid control prototyping for research and teaching," *HardwareX*, 2023, vol. 14, pp. 70–74.



Andrea Lauri (Graduate Student Member, IEEE) received the B.Sc. and M.S. degrees in electronics engineering in 2018 and 2022, respectively, from the University of Padova, Padova, Italy, where he is currently working toward the Ph.D. degree in mechatronics engineering.

His current research interests focus on modeling and control of grid-connected inverters in microgrids.



Davide Biadene (Member, IEEE) received the M.S. degree in electronics engineering and the Ph.D. degree in information engineering from the University of Padova, Padova, Italy, in 2014 and 2017, respectively.

He is currently a Research Fellow with the Department of Management and Engineering, University of Padova. He was a visiting Ph.D. student with the Power Electronic Systems Laboratory, Department of Information Technology and Electrical Engineering, ETH Zurich, Zurich, Switzerland, in 2016. His current research interests include dc–dc converters for renewables and energy storage devices.

Switzerland, in 2016. His current research interests include dc–dc converters for renewables and energy storage devices.



Tommaso Caldognetto (Senior Member, IEEE) received the M.S. (Hons.) degree in electronics engineering and the Ph.D. degree in information engineering from the University of Padova, Padova, Italy, in 2012 and 2016, respectively.

He is currently an Assistant Professor with the Department of Management and Engineering, University of Padova. His research interests include the control of grid-tied converters, microgrid architectures, converters for dc

nanogrids, and real-time simulation for power electronics applications.

Dr. Caldognetto has been an Associate Editor for the IEEE OPEN JOURNAL OF POWER ELECTRONICS since 2019.



Paolo Mattavelli (Fellow, IEEE) received the M.S. (Hons.) and Ph.D. degrees in electrical engineering from the University of Padova, Padova, Italy, in 1992 and 1995, respectively.

He is currently a Full Professor in Electronics with the University of Padova. His current Google scholar H-index is 86. His major research interests include analysis, modeling, and control of power converters, grid-connected converters for renewable energy systems and microgrids, and high-temperature and high-power-density power electronics.

high-power-density power electronics.

Dr. Mattavelli was an Associate Editor for IEEE TRANSACTIONS ON POWER ELECTRONICS from 2003 to 2012. He is a Co-Editor-in-Chief for the IEEE TRANSACTIONS ON POWER ELECTRONICS. From 2005 to 2010, he was the Industrial Power Converter Committee Technical Review Chair for IEEE TRANSACTIONS ON INDUSTRY APPLICATIONS. For terms 2003–2006, 2006–2009, and 2013–2015, he was a member-at-large of the IEEE Power Electronics Society's Administrative Committee. He was a recipient of the Prize Paper Award in IEEE TRANSACTIONS ON POWER ELECTRONICS in 2005, 2006, 2011, and 2012, and the 2nd Prize Paper Award at the IEEE Industry Applications Society Annual Meeting in 2007.

Open Access funding provided by 'Universit? degli Studi di Padova' within the CRUI CARE Agreement